Observation of the sub-100 fs population of a dark state in a thiobase mediating intersystem crossing

Rocío Borrego-Varillas [†#], Danielle C. Teles-Ferreira [‡#], Artur Nenov[§#], Irene Conti[§#], Lucia Ganzer[†], Cristian Manzoni[†], Marco Garavelli[*§], Ana Maria de Paula[*‡] and Giulio Cerullo[*†]

[†] IFN-CNR, Dipartimento di Fisica, Politecnico di Milano, Piazza Leonardo da Vinci 32, I-20133 Milano, Italy

[‡] Departamento de Física, Universidade Federal de Minas Gerais, 31270-901 Belo Horizonte-MG, Brazil

[§] Dipartimento di Chimica Industriale, Università degli Studi di Bologna, Viale del Risorgimento 4, I-40136 Bologna, Italy

Supporting Information Placeholder

ABSTRACT: We combine sub 30-fs broadband transient absorption spectroscopy in the ultraviolet with state-of-the-art quantum mechanics/molecular mechanics simulations to study the ultrafast excited-state dynamics of the sulfur-substituted nucleobase 4-thiouracil. We observe a clear mismatch between the timescales for the decay of the stimulated emission from the bright ππ* state (76±16 fs, experimentally elusive until now) and the build-up of the photoinduced absorption of the triplet state (225±30 fs). These data provide evidence that the intersystem crossing occurs via a dark state, which is intermediately populated on the sub 100 fs timescale. Nonlinear spectroscopy simulations, extrapolated from a detailed CASPT2/MM decay path topology of the solvated system together with an excited state mixed quantum-classical non-adiabatic dynamics, reproduce the experimental results and explain the experimentally observed vibrational coherences. The theoretical analysis rationalizes the observed different triplet build-up times of 4- and 2-thiouracil.

INTRODUCTION

Thiobases[1,2] are DNA or RNA nucleobases where an exocyclic carbonyl oxygen is replaced by a sulfur atom. They have attracted much attention in recent years due to their biological relevance and their increasing amount of applications[3]. They have been used to improve polymerase chain reaction for DNA/RNA replication[4,5] and as cross-linking chromophores for investigation of specific interactions between nucleic acids and proteins[6,7]. Thanks to their near-unity triplet yields they have been also demonstrated as potent chemotherapeutic agents[8–10] for the treatment of some types of non-malignant hyperproliferative skin conditions and cancers. Besides their practical applications, they provide an excellent model system to understand how a single atom substitution can modify the energy relaxation pathways of the canonical DNA/RNA nucleobases. In comparison to the canonical nucleobases, thiation causes a red-shift in the absorption spectrum to the 280-400 nm range, leading to remarkable changes in the photophysics[11–18]: while in DNA/RNA monomers excited state deactivation occurs on an ultrafast timescale through a high rate of $S_1 \rightarrow S_0$ internal conversion[19–21], the major relaxation pathway in thiobases is via the population of long-lived triplet states through intersystem crossing (ISC)[14] occurring on the sub-picosecond timescale.

Over the past decade major efforts, both experimental[12–16,22–28] and computational[12,16,23,24,27,29–39], have been made to gain deeper understanding of the energy relaxation pathways and triplet state formation mechanisms in thiobases. Computational studies have suggested that the bright ππ* state relaxes on the sub-100-fs timescale by means of a conical intersection (CI) to a dark singlet nπ* state, which acts as a doorway to the triplet manifold. Such mechanism has been proposed for a number of thiobases, including 2-thiouracil[23,24], 4-thiothymine[16], 2-thiothymine[31], 2,4-dithiothymine[32], 2-thiocytosine[36] and 6-thioguanine[30]. While the femtosecond dynamics of the triplet states formation through ISC have been measured[14,16,35], so far there has been a lack of ultrafast spectroscopy data with sufficiently high temporal resolution to access the time scale of population of the dark state, proposed theoretically, to mediate ISC. Molecular dynamics simulations suggest time scales for this process ranging from sub-100 fs[39] to several picoseconds[16].

Here we combine broadband transient absorption (TA) spectroscopy featuring a sub-30-fs instrumental response function in the ultraviolet (UV) with hybrid quantum mechanics/molecular mechanics (QM/MM) state-of-the-art computational tools to study the ultrafast photoinduced dynamics of 4-thiouracil. We provide experimental evidence, quantitatively supported by the computational results, that ISC occurs predominantly via a dark state of nπ* character, that is intermediately populated on the sub-100 fs timescale from the bright photoexcited ππ* state.

MATERIALS AND METHODS

Sample preparation. 4-Thiouracil (97% purity) was purchased from Sigma-Aldrich and used as received. A phosphate-buffered saline (PBS) solution was prepared by dissolving 0.15 g of sodium dihydrogen phosphate and 0.27 g of sodium hydrogen phosphate in 200 ml of ultrapure water to obtain a pH 7.4 and a concentration of 16 mM. The 4-thiouracil in PBS solution was prepared to obtain a concentration of 6 mM, resulting in an absorbance of 2 OD at the central pump wavelength. The steady-state absorption spectrum is provided in the Supporting Information (SI) section 3.

Experimental setup. TA spectra measurements were carried out on a home-made pump-probe setup, based on a regeneratively amplified Ti:Sapphire laser (Libra, Coherent) at 800 nm wavelength with 100 fs pulse duration and 1 kHz repetition rate. A detailed description of the system can be found in reference[40]. Briefly, a fraction of the laser beam is sent to a non-collinear optical parametric amplifier (NOPA) whose output covers a broad bandwidth in the visible range (520-720 nm). The visible pulse and a fraction of the fundamental pulse are focused and mixed on a 50-μm-thick Type II β-barium-borate crystal to generate UV light by sum frequency[41]. The spectrum of the so-generated UV pulse spans from 320 nm to 360 nm (Figure S7 of the SI). A two-dimensional spectral-shearing interferometry measurement[42] revealed a duration of 16 fs. In order to avoid photodamage of the sample and generation of solvated electrons by two-photon absorption from water, the pump energy was limited to 27 nJ (resulting in a fluence of ~340 $\mu J/cm^2$) and a flowing jet configuration (0.2 mm path length) was employed. The sample was flown at a typical rate of 40 rpm. A broadband probe is obtained through white light continuum generation by focusing either the fundamental beam or its second harmonic in a slowly moving CaF_2 plate. The white light spectrum extends respectively in the visible (350-670 nm) or in the ultraviolet range (250-380 nm). After the sample, the transmitted probe is sent to a spectrometer (SP2150 Acton, Princeton Instruments) and detected using a linear image sensor driven and read out by a custom-built electronic board (Stresing Entwicklungsburo GmbH). For each probe wavelength, the differential absorption (ΔA) is measured as a function of the pump-probe time delay. For the experiments reported, the measurements were performed with parallel pump and the probe polarizations. Experiments performed for crossed and magic angle (Θ=54.7°) polarizations did not show any significant change in the dynamics.

Global analysis. The acquisition of transient absorption spectra produces a 2D map of the differential absorption (ΔA) as a function of the wavelength and the time delay. A global analysis of the data, performed using the Glotaran software[43], allows for extracting the time constants governing the dynamics over the entire dataset. A two-dimensional (2D) Fourier transform of the residuals of the global fit was performed to study the excited-state coherent oscillations.

COMPUTATIONAL METHODS

Classical molecular dynamics. The 4-thiouracil starting geometry was obtained running a classical molecular dynamics simulation, using the AMBER 12 suite[44,45] with the ff10 force field. Periodic boundary conditions were applied to a 40 x 39 x 35 Å periodic box containing 1210 water molecules, described by the TIP3P force field[46]. The hydrogen-containing bonds were restrained by the SHAKE algorithm[47] while the water geometry was rigidized by the SETTLE scheme[48]. Non-bonding and electrostatic interactions were evaluated with a cutoff of 9 Å, making use of the particle mesh Ewald method for quantification of the long-range electrostatics. The time step was set to 0.5 fs and integration of the equations of motion was done with the leap-frog algorithm. Thermalization of the systems was reached by heating of the pre-optimized system to 300 K in 15 ps steps of 100 K. A production run at 300 K and 1 atm was carried out for 500 ps. The lowest energy structure along the dynamics was selected as a starting point for subsequent QM/MM refinement.

QM/MM calculations: geometry refinement and electronic structure computations. QM/MM calculations were executed with the COBRAMM program, developed in our group interfacing various QM codes with AMBER[49]. An High/Medium/Low layers partitioning was applied to a spherical droplet centered at 4-thiouracil with a radius of 12 Å (containing 245 waters), obtained from the cubic box. The QM region comprises the thionucleobase. The water molecules in 3 Å distance were included in the movable Medium (MM) layer. The remaining water molecules were kept fixed in the (MM) Low layer. Ground state geometry minimum was obtained at the Møller-Plesset second order perturbation theory (MP2) level. The geometry optimizations were computed at the MS-CASPT2[50] level, using an active space including the sulfur lone pair and the valence π-orbitals to a total of 12 electrons in 9 orbitals (Figure S6 in the SI). The ANO-L basis set was used[51], adopting contractions 5s4p2d1f on sulphur, 4s3p2d1f on carbon/oxygen/nitrogen and 3s2p1d on hydrogen atoms. State-average was performed over the lowest five states. The electronic structure at critical points was refined through a larger active space, extended by the lone pair of the oxygen and a pair of bonding and anti-bonding carbon-sulfur σ orbitals to a total of 16 electrons in 12 orbitals (Figure S6 in the SI), together with an enlarged ANO-RCC basis set[52], adopting the contractions 6s5p3d2f1g on sulphur, 5s4p3d2f1g on carbon/oxygen/nitrogen and 4s3p2d1f on hydrogen atoms contractions. Thereby, seven states were included in the state-averaging. The CASPT2 computations at critical points were performed both in the single-state and multi-state flavor. Thereby, the ionization-potential-electron-affinity (IPEA) shift[53] was set to 0.0 and an imaginary shift[54] of 0.2 a.u. was used throughout. The Cholesky decomposition was adopted in order to speed up the evaluation of two-electron integrals[56]. CI optimizations were performed with the gradient projection algorithm of Bearpark et al.[55] implemented in COBRAMM. All calculations were performed using the Molcas 8 package through its interface with COBRAMM[56].

Sampling and non-adiabatic mixed quantum-classical dynamics simulations. For each system 500 initial conditions were generated using the Wigner sampling technique through an interface with a stand-alone script, part of the quantum molecular dynamics program JADE[57], which considers temperature effects and mode-specific excitation. Consequently, sampling was performed at room temperature (300K). High frequency modes, belonging to C-H and N-H stretchings, were excluded from the sampling. Additionally, one normal mode with a very low frequency (< 100 cm^{-1}) was excluded from the sampling as it was asserted through preliminary sampling that displacement along this mode breaks the harmonic approximation and distorts excessively the geometry. Each realization was subjected to a 100 ps long MM equilibration run in which the QM region was kept fixed through harmonic constraints. This strategy allows the mobile MM region to adapt to each sampled geometry, thereby removing the bias of the water arrangement of the initial snapshot. The water coordinates of the last snapshot of the MM equilibration run were combined with the sampled thiouracil geometry to form the snapshot used to compute the electronic properties.

We recently documented a detailed study on the dependence of the linear absorption (LA) spectrum of 4-thiouracil on various parameters (active space, protocol (SS-CASPT2 vs. MS-CASPT2), basis set)[18]. Based on this study we conclude that the SS-RASPT2/SA-3-RASSCF(12,9|2,4) level of theory, comprising all valence π-orbitals, the lone pair of the sulfur and four extra-valence virtual orbitals with up to double excitations in the latter is best suited for the dynamics simulations due to the very good agreement between simulated and experimental LA spectra[18], whereas the full-valence active space red-shifts the absorption band of the lowest bright $\pi\pi^*$ state by 20 nm. 30 geometry realizations for which the $^1\pi\pi^*$ (S_2) transition falls under the envelope of the pump pulse (Figure S20 in the SI) were selected and for each a 180 fs long non-adiabatic mixed quantum-classical molecular dynamics simulation following Newton's equations of motion for the nuclei and utilizing hybrid QM/MM gradients was performed at the SS-RASPT2/SA-3-RASSCF(12,9|2,4) level of theory with a time step of 1.0 fs applying the Tully's fewest switches surface hopping algorithm[58] with the Tully-Hammes-Schiffer scheme[59] using the COBRAMM's parallel environment for computing nu-

merical gradients (details in the SI section 1.2). The state averaging covered the ground, the lowest (dark) $n\pi^*$ (S_1) and the lowest (bright) $\pi\pi^*$ states (S_2), and the dynamics was always initiated in the S_2 state. The movable (MM) water layer was extended to 5 Å to accommodate pronounced distortions of the aromatic ring.

Spectroscopy simulations. The ΔA signal was computed as the marginal (with respect to the delay time t_1) of the two-dimensional Fourier transform (with respect to t1 and t_3) of the nonlinear response of the system which becomes equal to the third-order signal within the limit of temporally well separated ultrashort laser pulses (impulsive limit). The non-linear response can be expressed within the framework of the cumulant expansion of Gaussian fluctuations (CGF)[60–62] (the working equations can be found in the SI section 1.3). It allows for calculating the shapes of electronic transition bands coupled to a bath for fluctuations with arbitrary time scales by using the formalism of lineshape functions when the fluctuations follow Gaussian statistics. The spectral diffusion is described via composite lineshape functions, consisting of a portion describing the vibrational progressions in the spectra, due to undamped molecular vibrations represented through the multidimensional uncoupled displaced harmonic oscillator (DHO)[61,63], and a portion describing the homogeneous broadening due to a coupling to a continuum of low-frequency modes, represented by the lineshape function of the semi-classical Brownian oscillator (OBO)[61,63,64]. DHO parameters necessary to describe the spectral dynamics were obtained from electronic structure calculations within the RASSCF/RASPT2 framework (see SI sections 1.3.4 and 1.3.5). OBO parameters were chosen so to reproduce the linear absorption spectrum of the $\pi\pi^*$ state at room temperature (Figure S7 in the SI). Further details are provided in the SI (section 1.3.6). Population relaxation processes are described by the Pauli master equation solved for a sequential model that describes the decay of the dominant part of the population via the path $S_2 \rightarrow S_1 \rightarrow T_1$ (section 1.3.2 in the SI). The secondary path $S_2 \rightarrow T_2 \rightarrow T_1$ was neglected in the simulations as it gives rise only to weak photoinduced absorption contributions. Spectra simulations were performed with a development version of Spectron 2.7.[62]

RESULTS AND DISCUSSION

Figure 1 shows the experimental (Figure A, B) and theoretical (Figure C, D) two-dimensional (2D) maps of the differential absorption (ΔA) signal of 4-thiouracil dissolved in a phosphate saline buffer (PSB) solution at pH 7.4. The upper panel in (A) shows the dynamics at 400 nm and 600 nm (dotted lines in the map) and the upper panel in (C) shows the calculated $S_2(\pi\pi^*)$ population decay. Immediately after the pump pulse, we observe a negative signal, which is assigned to the superposition of two bands: the tail of the ground state bleaching (GSB) band at 360 nm and a stimulated emission (SE) band peaking around 400 nm. The GSB is associated with depletion of the ground state after excitation of S_2. The SE is assigned to the bright S_2 state photoexcited by the pump ($\pi\pi^*$ transition). An additional excited state absorption (ESA) signature of S_2 at around 275 nm was found by probing in the UV (see SI section 4.5). The pump pulse populates the lowest $\pi\pi^*$ state in the Franck-Condon (FC) region. The vibrational dynamics in this bright state gives rise to intensity beats in the SE signal, whose central wavelength (400 nm) matches also the energy gap at the $\pi\pi^*$ state minimum (Min $\pi\pi^*$).

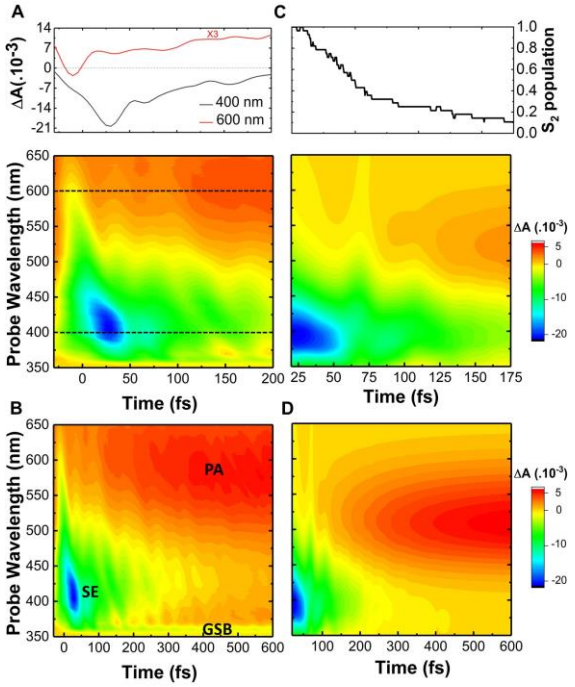

Figure 1. ΔA maps of 4-thiouracil in PBS solution. Experimental panels: A (short scale from -30 fs until 200 fs) and B (long scale from 30 fs until 600 fs). Simulated panels: C (short scale) and D (long scale). Upper panel in (A) shows the dynamics at 400 nm and 600 nm (dotted lines in the map), upper panel in (C) shows the calculated $S_2(\pi\pi^*)$ population decay.

Both the SE (Figure 1) and the ESA (Figures S24 and S25) bands associated with S_2 display a first ultrafast decay on the sub-100-fs timescale, which is followed by the delayed build-up of a photoinduced absorption (PA) band around 600 nm on the ~500 fs timescale. The dynamics at 400 nm and 600 nm are shown in Figure 1A. The PA band, whose build-up has been observed in previous studies with a lower 200-fs time resolution[14], has been assigned to triplet-triplet absorption, thus providing a fingerprint of the ISC. Following its formation, the PA band undergoes a blue-shift on the sub-picosecond timescale (Figure 2A), which is assigned to vibrational cooling of the long-lived[65,66] triplet state.

Our experimental data clearly show a mismatch between the decay time of the SE and the build-up time of the PA signal, thus delivering an experimental confirmation that ISC does not occur directly from the photoexcited bright $\pi\pi^*$ state but is predominantly mediated by an intermediate dark state as proposed by previous theoretical works[16,23,31-33,35,36,39].

Figure 2B shows the decay associated spectra (DAS) obtained by a global fit of the data, revealing time constants of 76±16 fs and 225±30 fs. The 76 fs time constant (black line) is attributed to the decay of the SE band. The 225 fs DAS band between 500 and 650 nm is associated to the subsequent triplet PA formation. A long living component was fixed as an offset to account for the decay beyond our time observation window. This offset is therefore related to the long-living triplet state.

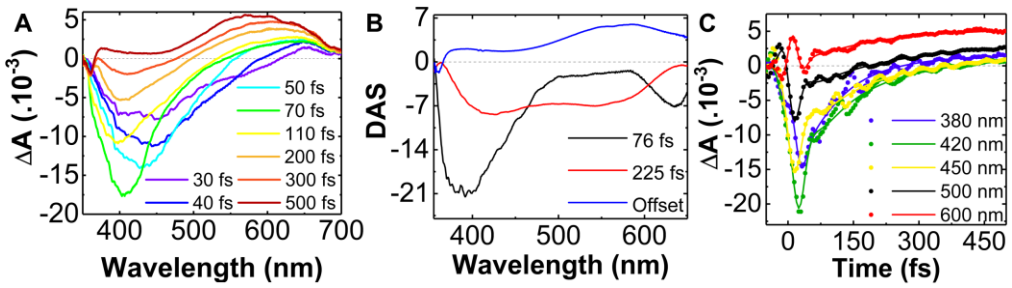

Figure 2. (A) ΔA spectra of 4-thiouracil at selected time delays. (B) DAS obtained by global analysis. (C) Dynamics at given wavelengths: experimental data (dots) fitted by a global analysis (solid line).

At all wavelengths the ΔA signal is modulated by a complex oscillatory pattern that is assigned to vibrational coherences impulsively excited by the sub-20-fs pump pulse (Figure 2 C).To extract the frequencies of the observed coherent oscillations we perform a 2D Fourier analysis of the oscillatory component of the spectra. To separate this component we subtract from the experimental data the exponential decay part obtained from the fit (see more details in SI). Figure 3 A shows the obtained 2D map showing two modes with frequencies of 680 cm^{-1} and 400 cm^{-1}, that are in agreement with the Fourier transform of the simulated spectra. To shed light into the underlying molecular deformations we run a limited ensemble of 30 room temperature trajectories employing Tully's fewest switches surface hopping algorithm (see SI Figures S9-S12, a representative trajectory depicted in the lower panel of Figure 4). A decomposition of the ground state-ππ* energy gap dynamics along each trajectory into contributions from the individual normal modes within the framework of the DHO model (SI, section 2.5) allows for identifying the normal modes responsible for the coherent beatings of the SE. In particular, we observe coherent dynamics in the 457 cm^{-1} breathing mode and in two hydrogen-out-of-plane (HOOP) bending modes with frequencies 697 cm^{-1} and 784 cm^{-1} (Figure 3B), in good agreement with the experimentally observed frequencies. We associate both HOOP modes with the 680 cm^{-1} frequency in the 2D Fourier transform.

The population of the ππ* singlet state is ballistically driven towards the nπ* singlet state through a sloped CI separated from the minimum by ca. 0.2 eV barrier (Figure 4). The population decay dynamics (Figure 1C) is fitted with a time constant of 67.5 fs in agreement with the 76 fs time constant extracted from the global analysis. This ultrafast decay is remarkable considering the relatively large S_2/S_1 energy gap of 1.0 eV at the S_0 equilibrium. We note, however, that already the sampling of vibrational degrees of freedom in the 330-360 nm pump window decreases the S_2/S_1 gap to about 0.5 eV (see Figure S8). The molecular dynamics simulations show that the access to the CI seam is facilitated through bond stretching deformations (mainly C_5-C_6 and C_4-S elongation) and occurs in half of the trajectories within one to two periods of the oscillation (section 2.3 in the SI). Thereby, the ππ*/nπ* crossings are characterized by significantly elongated C_5-C_6 and C_4-S bond lengths, with values well beyond the ππ* equilibrium (Figure S19 in the SI). Consequently, 4-thiouracil does not have time to redistribute the energy into out-of-plane modes during the ultrashort life span of the S_2 state. This scenario is supported by the very good agreement between theory and experiment regarding the vibrational features extracted out of the TA spectra (Figure 3A). The only vibrational modes below 1200 cm^{-1} observed experimentally could be unequivocally assigned to ring breathing and hydrogen out-of-plane vibrations, which preserve the planarity of the ring. The lack of further vibrational signatures in the 2D Fourier transform maps suggests that no ring-distortion modes, which would carry their characteristic frequencies, are involved. The in-plane decay mechanism is in line with the results of CASPT2 dynamics simulations by Mai et al.[39] on 2-thiouracil, who also report a sub-100 fs ππ* life time originating from competing $S_2 \rightarrow S_1 \rightarrow T_1$ and $S_2 \rightarrow T_2 \rightarrow T_1$ pathways, the former being more efficient (ca. 75%). On the contrary, semi-empirical simulations on the closely related 5-methyl-4-thiouracil see ring-twisting deformations, which occur on a picosecond time scale, essential for reaching the ππ*→nπ* crossing seam[16].

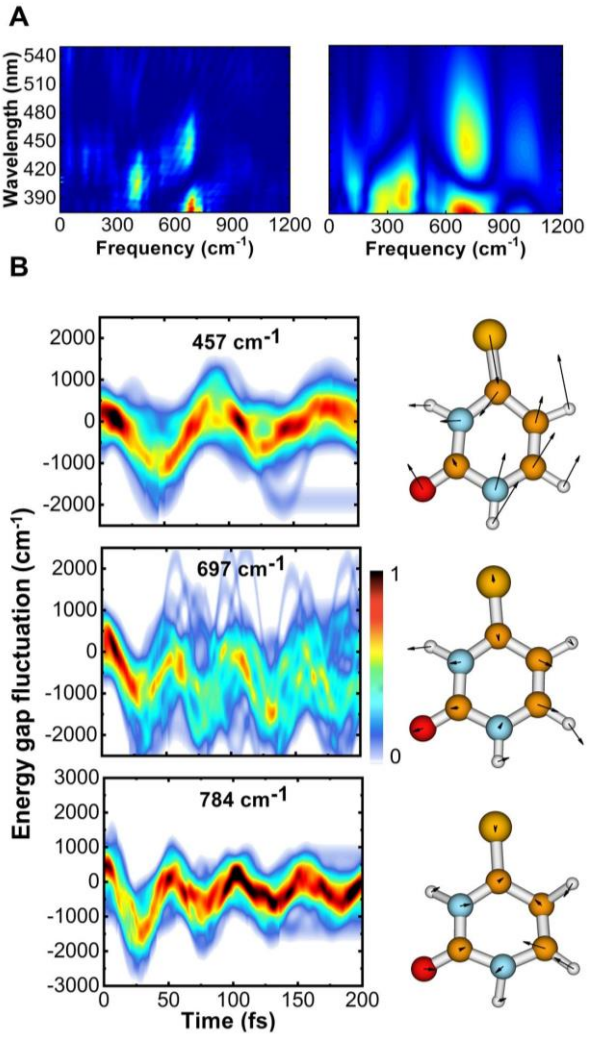

Figure 3. (A) 2D Fourier transform of the residuals of the experimental (left) and theoretical (right) ΔA dynamics. (B) Coherent energy gap fluctuations along selected vibrational modes at 457 cm^{-1} (ring breathing), 697 cm^{-1} (H7 and H11 hydrogen-out-of-plane (HOOP) bending) and 784 cm^{-1} (H7, H11 and H12 out-of-plane). The breathing mode gives rise to the 400 cm^{-1} peak in the 2D Fourier transforms, while both HOOP modes are responsible for the 680 cm^{-1} peaks. Intensities associated with trajectory density.

Table 1. Energetics (nm) and oscillator strength of electronic states giving rise to stimulated emission (red) and photoinduced absorption (blue) out of the corresponding electronic state indicated on top of each column. Computations were performed at the SS-CASPT2/SA-CASSCF(16,12)/ANO-RCC level averaging over 30 states.

	Min S_0 (S_2)	Min $n\pi^*$ (S_1)	Min $\pi\pi^*$ (S_2)	Min $^3\pi\pi^*$ (T_1)	Min $^3n\pi^*$ (T_2)
Absorption bands and oscillator strengths	341 (0.42)	376 (0.02)	415 (0.28)	599 (0.02)	617 (0.02)
	469 (0.01)	279 (0.01)	765 (0.01)	534 (0.01)	397 (0.01)
	379 (0.01)	246 (0.01)	355 (0.08)	335 (0.02)	349 (0.03)
	378 (0.04)		284 (0.08)	327 (0.01)	343 (0.01)
	312 (0.01)		259 (0.01)	308 (0.01)	330 (0.01)
	295 (0.11)		256 (0.09)	299 (0.01)	285 (0.04)
	290 (0.01)		245 (0.01)	273 (0.05)	244 (0.05)
	282 (0.03)			250 (0.01)	241 (0.01)
	268 (0.04)			243 (0.03)	
	267 (0.02)				
	267 (0.04)				

Upon decay to the nπ* state the high frequency stretching modes exhibit partial damping on the 180 fs time scale of the simulation, whereas low frequency ring-puckering modes are activated (see Figure S16 in the SI) and the system can explore regions beyond the planar minimum (Min nπ* in Figure 4). Virtually everywhere on the accessible nπ* potential energy surface the nπ* is found to be isoenergetic with two triplet states, of ^{3}nπ* and of ^{3}ππ* nature, respectively (black and red diamond labels in Figure 4). Hence, the nπ* state acts as a doorway for the effective population of the triplet manifold. The ^{1}nπ*/^{3}ππ* ISC is facilitated by a 160 cm^{-1} spin-orbit coupling. The longer time constant of 225 fs is assigned to the build-up of the PA from the ^{3}ππ* triplet state around 600 nm (Figure 1B), supported by our static computations revealing higher lying states in the triplet manifold (marked in blue in Figure 4) being the source of a PA around 525 nm in the simulated spectra (Figure 1D). We note that the ^{1}nπ* state is completely dark in the probed spectral window as it exhibits only one weak PA signal at 376 nm which falls under the much more intense GSB/SE band. While we cannot make a conclusive assignment for the 400-425 nm band present in the 225 fs DAS, we propose two possible explanations for this band. One is a small component of S_2 population unable to reach the CI seam, which remains in S_2 for a longer time giving rise to a residual SE signal. Another possibility is the population of the T_2 triplet state, which is nearly degenerate with T_1. As it can be seen in Table 1, T_2 presents ESA signal at 397 nm which could contribute to the 400-425 nm peak in the 225 fs DAS and to the positive component in the offset DAS in the same wavelength region.

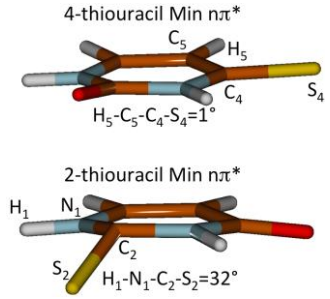

Scheme 1 Structures of the ^{1}nπ* minima (Min ^{1}nπ*) in 4- and 2-thiouracil

In the present work the presence of the possible secondary decay channel $S_2(^1\pi\pi^*)\rightarrow T_2(^3n\pi^*)\rightarrow T_1(^3\pi\pi^*)$ (involving at least 13-25% of the population[16,31]) is mapped only statically at the QM/MM level (dashed grey arrows in Figure 4). While at the S_2 minimum the S_2/T_2 and S_2/T_1 energy gaps are rather large (0.8-1.0 eV), thus making an ISC rather inefficient in this region, the S_2/T_2 energy gap is significantly reduced in the vicinity of the S_2/S_1 CI crossing (0.2 eV). Furthermore, we obtain a large S_2/T_2 spin-orbit coupling of 140 cm^{-1} rationalized by the different nature of the two states. The involvement of the $S_2\rightarrow T_2\rightarrow T_1$ path is supported by the peak at 600-650 nm observed in the DAS (Figure 2B) with the fast time constant (76 fs). This peak coincides with the PA from the T_2 minimum (~620 nm, see Table 1), which builds up concomitantly with the S_2 decay, revealing that $S_2\rightarrow T_2$ intersystem crossing could take place at the same time scale of the non-adiabatic $S_2\rightarrow S_1$ transition. In a joint experimental/theoretical study on 4-thiothymine[16] the authors also report a three-state ($S_2/S_1/T_2$) quasi-degenerate region and suggest, based on dynamics simulations, that 13% of the population undergoes the $S_2\rightarrow T_2\rightarrow T_1$ path. Simulations on 2-thiouracil predict 25% of the population to populate this secondary channel. The subsequent T_1 ($^3\pi\pi^*$) population (from the Min ^{3}nπ*) occurs at longer lifetimes (~225 fs), as documented by the peak around 550 nm assigned to the PA of the T_1 state (see Table 1).

Notably, we measure an ISC time in 4-thiouracil which is about two times faster as compared to 2-thiouracil. Pollum et al.[14] measured a triplet build-up time of 360 fs for 2-thiouracil, in agreement with our results on 2-thiouracil of ≈400 fs (see Figure S26 in the SI)[67]. According to our calculations, there are two possible explanations for this behavior. On one side, the minimum on the nπ* state in 4-thiouracil is planar in contrast to 2-thiouracil (see Scheme 1), which exhibits an out-of-plane bending of the sulfur[23,24], also characteristic for nucleobases[23,47,48] . On the other side, in 4-thiouracil the nπ* minimum coincides with the ISC, whereas in 2-thiouracil a barrier of ca. 0.1 eV has to be overcome[23,24] (see SI).

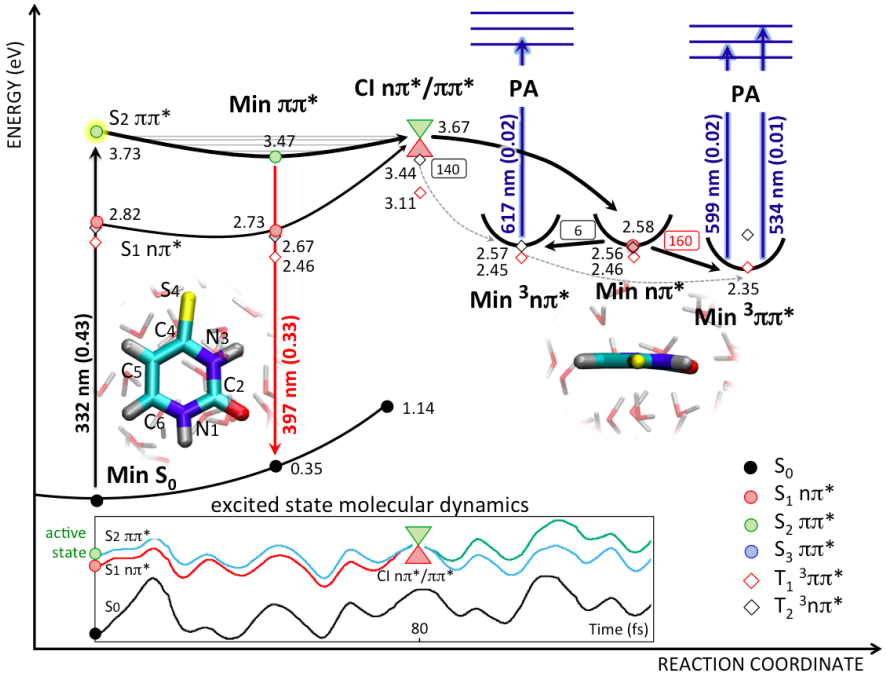

Figure 4. CASPT2/MM decay path from the lowest ππ* bright state (S_2 at the FC point) of 4-thiouracil in water. Vertical black arrow indicates the absorption wavelength of the lowest bright state S_2 at the FC point. Red arrow indicates the stimulated emission out of the minimum on the lowest ππ* bright state. Blue arrows indicate the photo-induced absorption from the triplet minima, giving rise to the excited state absorption band between 500 nm and 650 nm in the transient absorption spectra (see Figure 1 B,D). Dashed grey arrows show the secondary decay path involving $S_2 \rightarrow T_2 \rightarrow T_1$ transitions. Spin-orbit couplings are highlighted in text boxes. Inset: a representative trajectory of non-adiabatic molecular dynamics showing the energies of the electronic states – ground (S_0, black), nπ* (S1, red) and ππ* (S_2, green) – at the geometries sampled along the dynamics. The "active" state, i.e. the state responsible for the quantum feedback on the nuclei is shown in light blue. The dynamics is initiated in the S_2 state (i.e. the initial vibrational dynamics is driven by the potential energy surface of the ππ* state), after ca. 80 fs, it reaches the CI through which it decays to S_1.

CONCLUSION

In conclusion, high time resolution transient absorption spectroscopy in the UV range allowed us to observe for the first time an ultrafast (sub-100-fs) decay component in the photoinduced dynamics of 4-thiouracil following excitation of its bright ππ* state, which does not match the build-up time of the fingerprint signals of the triplet states. This is a proof of the involvement of intermediate dark states, mainly the ^{1}nπ*, acting as doorway to the triplet manifold. This interpretation is supported by high-level *ab-initio* static and dynamic numerical modeling, which allows us also to characterize the leading vibrational modes responsible for the experimentally observed coherences. In addition, the modeling is able to rationalize the faster triplet population in 4-thiouracil compared to its isomer 2-thiouracil.

ASSOCIATED CONTENT

Supporting Information

Materials and steady-state spectroscopy; description of the experimental setup; transient spectra; dynamics; global analysis; coherent oscillations; details on the QM/MM protocol; details on the non-adiabatic mixed quantum-classical dynamics simulations; theoretical background of nonlinear spectroscopy; protocols for acquisition of the simulation parameters; electronic structures at representative geometries; active space orbitals; trajectory plots; normal mode analysis; Cartesian coordinates.

AUTHOR INFORMATION

Corresponding Author

* marco.garavelli@unibo.it
* ana@fisica.ufmg.br
* giulio.cerullo@polimi.it

Author Contributions

# These authors equally contributed to this work.

Notes

The authors declare no competing financial interests.

ACKNOWLEDGMENT

This work was supported by the European Research Council Advanced Grant STRATUS (ERC-2011-AdG No. 291198), the Marie Curie actions (FP7-PEOPLE-IEF-2012) and the H2020 Grant Agreement number 765266 (LightDyNAmics). DCTF and AMdP acknowledge financial support from the funding agencies Fapemig, CNPq and CAPES. We thank Dr. Stefano Santabarbara for preparing the PBS.

REFERENCES

(1) Ashwood, B.; Pollum, M.; Crespo-Hernández, C. E. *Photochem. Photobiol.* **2018**, 0–2.
(2) Arslancan, S.; Martínez-Fernández, L.; Corral, I. *Molecules* **2017**, *22* (6).
(3) Pollum, M.; Martínez-Fernández, L.; Crespo-Hernández, C. E. In *Top Curr Chem*; Springer, 2014; pp 245–327.
(4) Sismour, A. M. *Nucleic Acids Res.* **2005**, *33* (17), 5640–5646.
(5) Heuberger, B. D.; Pal, A.; Del Frate, F.; Topkar, V. V.; Szostak, J. W. *J. Am. Chem. Soc.* **2015**, *137* (7), 2769–2775.
(6) Meisenheimer, K. M.; Koch, T. H. *Crit. Rev. Biochem. Mol. Biol.* **1997**, *32* (2), 101–140.
(7) Favre, A.; Moreno, G.; Blondel, M. O.; Kliber, J.; Vinzens, F.;

Salet, C. *Biochem. Biophys. Res. Commun.* **1986**, *141* (2), 847–854.
(8) Pollum, M.; Jockusch, S.; Crespo-Hernández, C. E. *J. Am. Chem. Soc.* **2014**, *136* (52), 17930–17933.
(9) Reelfs, O.; Karran, P.; Young, A. R. *Photochem. Photobiol. Sci.* **2012**, *11* (1), 148–154.
(10) Pollum, M.; Lam, M.; Jockusch, S.; Crespo-Hernández, C. E. *ChemMedChem* **2018**, *13* (10), 1044–1050.
(11) Reichardt, C.; Crespo-Hernaíndez, C. E. *J. Phys. Chem. Lett.* **2010**, *1* (15), 2239–2243.
(12) Reichardt, C.; Guo, C.; Crespo-Hernández, C. E. *J. Phys. Chem. B* **2011**, *115* (12), 3263–3270.
(13) Pollum, M.; Crespo-Hernández, C. E. *J. Chem. Phys.* **2014**, *140* (7).
(14) Pollum, M.; Jockusch, S.; Crespo-Hernández, C. E. *Phys. Chem. Chem. Phys.* **2015**, *17* (41), 27851–27861.
(15) Ashwood, B.; Jockusch, S.; Crespo-Hernández, C. E. *Molecules* **2017**, *22* (3).
(16) Martínez-Fernández, L.; Granucci, G.; Pollum, M.; Crespo-Hernández, C. E.; Persico, M.; Corral, I. *Chem. - A Eur. J.* **2017**, *23* (11), 2619–2627.
(17) Nenov, A.; Borrego-Varillas, R.; Oriana, A.; Ganzer, L.; Segatta, F.; Conti, I.; Segarra-Marti, J.; Omachi, J.; Dapor, M.; Taioli, S.; et al. *J. Phys. Chem. Lett.* **2018**, *9* (7), 1534–1541.
(18) Nenov, A.; Conti, I.; Borrego-Varillas, R.; Cerullo, G.; Garavelli, M. *Chem. Phys. (Under Revis.* **2018**.
(19) Middleton, C. T.; de La Harpe, K.; Su, C.; Law, Y. K.; Crespo-Hernández, C. E.; Kohler, B. *Annu. Rev. Phys. Chem.* **2009**, *60* (1), 217–239.
(20) Crespo-Hernández, C. E.; Cohen, B.; Hare, P. M.; Kohler, B. *Chem. Rev.* **2004**, *104* (4), 1977–2019.
(21) Pecourt, J. M. L.; Peon, J.; Kohler, B. *J. Am. Chem. Soc.* **2000**, *122* (38), 9348–9349.
(22) Harada, Y.; Okabe, C.; Kobayashi, T.; Suzuki, T.; Ichimura, T.; Nishi, N.; Xu, Y. Z. *J. Phys. Chem. Lett.* **2010**, *1* (2), 480–484.
(23) Mai, S.; Marquetand, P.; González, L. *J. Phys. Chem. Lett.* **2016**, *7* (11), 1978–1983.
(24) Mai, S.; Marquetand, P.; González, L. *J. Phys. Chem. A* **2015**, *119* (36), 9524–9533.
(25) Sánchez-Rodríguez, J. A.; Mohamadzade, A.; Mai, S.; Ashwood, B.; Pollum, M.; Marquetand, P.; González, L.; Crespo-Hernández, C. E.; Ullrich, S. *Phys. Chem. Chem. Phys.* **2017**, *19* (30), 19756–19766.
(26) Yu, H.; Sanchez-Rodriguez, J. A.; Pollum, M.; Crespo-Hernández, C. E.; Mai, S.; Marquetand, P.; González, L.; Ullrich, S. *Phys. Chem. Chem. Phys.* **2016**, *18* (30), 20168–20176.
(27) Jiang, J.; Zhang, T. S.; Xue, J. D.; Zheng, X.; Cui, G.; Fang, W. H. *J. Chem. Phys.* **2015**, *143* (17).
(28) Koyama, D.; Milner, M. J.; Orr-Ewing, A. J. *J. Phys. Chem. B* **2017**, *121* (39), 9274–9280.
(29) Bai, S.; Barbatti, M. *J. Phys. Chem. A* **2016**, *120* (32), 6342–6350.
(30) Martínez-Fernández, L.; Corral, I.; Granucci, G.; Persico, M. *Chem. Sci.* **2014**, *5* (4), 1336.
(31) Cui, G.; Fang, W. *J. Chem. Phys.* **2013**, *138* (4), 044315.
(32) Xie, B.-B.; Wang, Q.; Guo, W.-W.; Cui, G. *Phys. Chem. Chem. Phys.* **2017**, *19* (11), 7689–7698.
(33) Zou, X.; Dai, X.; Liu, K.; Zhao, H.; Song, D.; Su, H. *J. Phys. Chem. B* **2014**, *118* (22), 5864–5872.
(34) Gobbo, J. P.; Borin, A. C. *Comput. Theor. Chem.* **2014**, *1040–1041*, 195–201.
(35) Reichardt, C.; Crespo-Hernández, C. E. *Chem. Commun.* **2010**, *46* (32), 5963.
(36) Mai, S.; Pollum, M.; Martínez-Fernández, L.; Dunn, N.; Marquetand, P.; Corral, I.; Crespo-Hernández, C. E.; González, L. *Nat. Commun.* **2016**, *7* (May), 13077.
(37) Mai, S.; Ashwood, B.; Marquetand, P.; Crespo-Hernández, C. E.; González, L. *J. Phys. Chem. B* **2017**, *121* (20), 5187–5196.
(38) Martinez-Fernandez, L.; Fahleson, T.; Norman, P.; Santoro, F.; Coriani, S.; Improta, R. *Photochem. Photobiol. Sci.* **2017**, *16* (9), 1415–1423.
(39) Ruckenbauer, M.; Mai, S.; Marquetand, P.; González, L. *J. Chem. Phys.* **2016**, *144* (7), 0–8.
(40) Borrego-Varillas, R.; Ganzer, L.; Cerullo, G.; Manzoni, C. *Appl. Sci.* **2018**, *8* (6), 989.
(41) Varillas, R. B.; Candeo, A.; Viola, D.; Garavelli, M.; Silvestri, S. De; Cerullo, G.; Manzoni, C.; De Silvestri, S.; Cerullo, G.; Manzoni, C.; et al. *Opt. Lett.* **2014**, *39* (13), 3849–3852.
(42) Borrego-Varillas, R.; Oriana, A.; Branchi, F.; De Silvestri, S.; Cerullo, G.; Manzoni, C. *JOSA B* **2015**, *32* (9), 1851–1855.
(43) Snellenburg, J. J.; Laptenok, S. P.; Seger, R.; Mullen, K. M.; Stokkum, I. H. M. van. *J. Stat. Softw.* **2012**, *49* (3).
(44) Case, D. A.; Darden, T.; Cheatham, T. E.; Simmerling, C.; Wang, J.; Duke, R. E.; Luo, R.; Walker, R. C.; Zhang, W.; Merz, K. M.; et al. *Univ. California, San Fr.* **2012**, 350.
(45) Salomon-Ferrer, R.; Case, D. A.; Walker, R. C. *Wiley Interdiscip. Rev. Comput. Mol. Sci.* **2013**, *3* (2), 198–210.
(46) Jorgensen, W. L.; Chandrasekhar, J.; Madura, J. D.; Impey, R. W.; Klein, M. L. *J. Chem. Phys.* **1983**, *79* (2), 926–935.
(47) Ryckaert, J. P.; Ciccotti, G.; Berendsen, H. J. C. *J. Comput. Phys.* **1977**, *23* (3), 327–341.
(48) Miyamoto, S.; Kollman, P. A. *J. Comput. Chem.* **1992**, *13* (8), 952–962.
(49) Weingart, O.; Nenov, A.; Altoè, P.; Rivalta, I.; Segarra-Martí, J.; Dokukina, I.; Garavelli, M. *J. Mol. Model.* **2018**, *24* (9), 271.
(50) Finley, J.; Malmqvist, P.-Å.; Roos, B. O.; Serrano-Andrés, L. *Chem. Phys. Lett.* **1998**, *288* (2–4), 299–306.
(51) Widmark, P.-O.; Malmqvist, P.-A.; Roos, B. O. *Theor. Chim. Acta* **1990**, *77* (5), 291–306.
(52) Roos, B.; Lindh, R.; Malmqvist, P.-Å.; Veryazov, V.; Widmark, P.-O. *J. Phys. Chem. A* **2004**, *108* (15), 2851–2858.
(53) Ghigo, G.; Roos, B. O.; Malmqvist, P.-Å. *Chem. Phys. Lett.* **2004**, *396* (1–3), 142–149.
(54) Forsberg, N.; Malmqvist, P.-Å. *Chem. Phys. Lett.* **1997**, *274* (1–3), 196–204.
(55) Bearpark, M. J.; Robb, M. A.; Bernhard Schlegel, H. *Chem. Phys. Lett.* **1994**, *223* (3), 269–274.
(56) Aquilante, F.; Autschbach, J.; Carlson, R. K.; Chibotaru, L. F.; Delcey, M. G.; De Vico, L.; Fdez. Galván, I.; Ferré, N.; Frutos, L. M.; Gagliardi, L.; et al. *J. Comput. Chem.* **2016**, *37* (5), 506–541.
(57) Du, L.; Lan, Z. *J. Chem. Theory Comput.* **2015**, *11* (4), 1360–1374.
(58) Tully, J. C. *Faraday Discuss.* **1998**, *110*, 407–419.
(59) Hammes-Schiffer, S.; Tully, J. C. *J. Chem. Phys.* **1994**, *101* (6), 4657–4667.
(60) Mukamel, S.; Abramavicius, D. *Chem. Rev.* **2004**, *104* (4), 2073–2098.
(61) Mukamel, S. *Principles of Nonlinear Optical Spectroscopy*; Oxford University Press on Demand, 1999.
(62) Abramavicius, D.; Palmieri, B.; Voronine, D. V.; Šanda, F.; Mukamel, S. *Chem. Rev.* **2009**, *109* (6), 2350–2408.
(63) Li, B.; Johnson, A. E.; Mukamel, S.; Myers, A. B. *J. Am. Chem. Soc.* **1994**, *116* (24), 11039–11047.
(64) Butkus, V.; Valkunas, L.; Abramavicius, D. *J. Chem. Phys.* **2012**, *137* (4), 044513.
(65) Bai, S.; Barbatti, M. *Phys. Chem. Chem. Phys.* **2017**, *19* (20), 12674–12682.
(66) Taras-Goślińska, K.; Wenska, G.; Skalski, B.; Maciejewski, A.; Burdziński, G.; Karolczak, J. *J. Photochem. Photobiol. A Chem.* **2004**, *168* (3), 227–233.
(67) A detailed investigation of the 2-thiouracil ultrafast excited-state dynamics will be presented in a forthcoming contribution that is in preparation process.
(68) Pepino, A. J.; Segarra-Martí, J.; Nenov, A.; Improta, R.; Garavelli, M. *J. Phys. Chem. Lett.* **2017**, *8* (8), 1777–1783.
(69) Conti, I.; Garavelli, M. *J. Phys. Chem. Lett.* **2018**, *9* (9), 2373–2379.
(70) Conti, I.; Martínez-Fernández, L.; Esposito, L.; Hofinger, S.; Nenov, A.; Garavelli, M.; Improta, R. *Chem. - A Eur. J.* **2017**, *23* (60), 15177–15188.

TABLE OF CONTENT FIGURE